Natural convection heat transfer simulation using energy conservative dissipative particle dynamics

Eiyad Abu-Nada*

Institut für Technische Verbrennung, Leibniz Universität Hannover, Welfengarten 1a, 30167 Hannover, Germany
and Department of Mechanical Engineering, Hashemite University, Zarqa 13115, Jordan
(Received 1 January 2010; published 18 May 2010)

Dissipative particle dynamics with energy conservation (eDPD) was used to study natural convection via Rayleigh-Bénard (RB) problem and a differentially heated enclosure problem (DHE). The current eDPD model implemented the Boussinesq approximation to model the buoyancy forces. The eDPD results were compared to the finite volume solutions and it was found that the eDPD method predict the temperature and flow fields throughout the natural convection domains properly. The eDPD model recovered the basic features of natural convection, such as development of plumes, development of thermal boundary layers, and development of natural convection circulation cells (rolls). The eDPD results were presented via temperature isotherms, streamlines, velocity contours, velocity vector plots, and temperature and velocity profiles. Further useful quantities, such as Nusselt number was calculated from the eDPD results and found to be in good agreement with the finite volume calculations.

I. INTRODUCTION

Dissipative particle dynamics (DPD) thermostat is a particle-based mesoscopic simulation method introduced by Hoogerbrugge and Koelman [1,2]. The DPD thermostat can predict complex hydrodynamics at mesoscale with a much higher computational efficiency compared to MD as each DPD particle represents a group or packet of actual molecules [3–7]. Español [8] and Avalos and Mackie [9] launched energy conservative DPD version appropriate for heat transport by introducing internal energy to the DPD system. The energy conservative DPD system is known in literature as eDPD. More recently, Pastewka *et al.* [10] introduced a Markov process for particle hydrodynamics with energy conservation that is equivalent to eDPD in the limit of a vanishing time step. Basically, in any eDPD model, each particle is prescribed by internal energy in addition to other quantities found in typical DPD thermostat models (mass, position, and velocity). Therefore, the heat transfer can be represented by the change of eDPD particles internal energy.

Since its introduction, the eDPD approach received little attention in the heat transfer community and its application was limited to relatively few heat transfer studies. For example, Ripoll *et al.* [11] and Ripoll and Español [12] studied heat transfer in one-dimensional (1D) heat conduction domain and their results were compared to analytical solution of the heat equation and good agreement was reported. Mackie *et al.* [13] applied the eDPD approach to model heat flow. More recently, the eDPD method was applied to simulate heat conduction in nanocomposites by Qiao and He [14] and heat conduction in nanoparticles suspensions by He and Qiao [15]. Also, Chaudhri and Lukes [16] extended the eDPD formulation to multicomponents and applied it to two-dimensional (2D) heat conduction. Recently, Abu-Nada [17] implemented different types of boundary conditions to 2D heat conduction domain using eDPD method and benchmarked the eDPD results against analytical and finite difference solutions.

As compiled from the above literature search, the eDPD studies available in literature that model heat flow (convective heat transfer) are still limited and it is very important to apply eDPD to fundamental problems of convection heat transfer as a first step toward promoting eDPD approach as a power tool that could mimic convective heat transfer at the mesoscale level. Besides, emerging fields in heat transfer such as heat transfer enhancement using nanofluids demands appropriate simulation tools that could explain mechanisms of convective heat transfer at the mesoscale level. For example, the effect of using nanoparticles in enhancing heat transfer in natural convection applications is still controversial in literature due to the contradiction between the experimental findings and the simulation results [18]. This controversy demands more robust simulation tools that could explain and predict mechanisms of heat transfer at the mesoscale level convection.

Up to the best knowledge of the current author, the only work in literature that applied eDPD to convection heat transfer is the work of Mackie *et al.* [13]. In their work, they applied the eDPD approach to simulate natural convection in a differentially heated enclosure (DHE). While they were successful in demonstrating part of the basic features of natural convection at low Rayleigh number, such as prediction of single circulation cell in the enclosure, but there are serious concerns about their results.

The first concern is that they simulated only a single case of natural convection at low Rayleigh where it was reported around Ra=10^3 without specifying the exact Rayleigh number. However, a closer look at their simulations (shown in Figs. 4 and 5 in their manuscript) reveals that the temperature isotherms resemble a Rayleigh number less than 10^3 (around 200) since the plotted isotherms were highly straighten up. Second, their simulations show nonsymmetric vector plots in the flow domain which completely contradicts

*Corresponding author; eiyad@hu.edu.jo

the basic theory of natural convection in enclosures, at low Rayleigh number, where a symmetric velocity profile have to prevail due to the domination of diffusion effects over convection effects. Also, the location of circulation cell was closer to the cold wall where in reality, for this low Rayleigh number, the location must be exactly at the center of the enclosure, which indicates huge density variation in their simulations (they related this to the compressibility of their model). Third, they show only qualitative description and no benchmarking against experimental or finite element/finite volume solutions were carried out. Therefore, there is a need to test eDPD model quantitatively in convective heat transfer applications and to be able to recover the basic features of natural convection, such as prediction of thermal boundary layers, prediction of the size and shape of the circulation cell (rolls), and development of thermal plumes.

Consequently, the objective of the present work is to apply eDPD to investigate natural convection heat transfer via two basic problems that are widely used in literature to study natural convection, which are Rayleigh-Bénard (RB) problem and DHE problem toward a better understanding of the application of eDPD method to model convective heat transfer problems. The present eDPD simulations will be benchmarked against finite volume solutions to assess the accuracy of the eDPD simulations.

II. eDPD GOVERNING EQUATIONS

Basically, similar to the typical DPD thermostat, the eDPD method is a particle method based on pairwise interactions between a particle and neighboring particles within a cutoff radius. The eDPD particles are still considered as a coarse-grained particle where each eDPD particle resembles a group of actual fluid molecules. The time progress of eDPD particles is governed by conservation of momentum and energy and is described by the following set of equations by absorbing the Boussinesq approximation,

$$\frac{d\vec{r}_i}{dt} = \vec{v}_i, \tag{1}$$

$$\frac{d\vec{v}_i}{dt} = (\vec{f}_{ij}^C + \vec{f}_{ij}^D + \vec{f}_{ij}^R) + \vec{g}\beta(T - T_o), \tag{2}$$

$$C_v \frac{dT_i}{dt} = (q_{ij}^{visc} + q_{ij}^{cond} + q_{ij}^R), \tag{3}$$

where β is the thermal expansion coefficient and $\vec{g}$ is the gravity vector. The conservative force $\vec{f}_{ij}^C$, dissipative force $\vec{f}_{ij}^D$ and random force $\vec{f}_{ij}^R$ are expressed as [[3–7,14,17]],

$$\vec{f}_{ij}^C = \sum_{j \neq i} a_{ij} w(r_{ij}) \vec{e}_{ij}, \tag{4}$$

$$\vec{f}_{ij}^D = \sum_{j \neq i} -\gamma_{ij} w^2(r_{ij})(\vec{e}_{ij} \cdot \vec{v}_{ij}) \vec{e}_{ij}, \tag{5}$$

$$\vec{f}_{ij}^R = \sum_{j \neq i} \sigma_{ij} w(r_{ij}) \zeta_{ij} \Delta t^{-1/2} \vec{e}_{ij}. \tag{6}$$

Also, the heat flux vectors q_{ij}^{cond}, q_{ij}^{visc}, q_{ij}^R accounts for viscous, collision, and random heat fluxes respectively and are given by [14,15,17]

$$q_{ij}^{cond} = \sum_{j \neq i} \kappa_{ij} w^2(r_{ij}) \left(\frac{1}{T_i} - \frac{1}{T_j} \right), \tag{7}$$

$$q_{ij}^{visc} = \sum_{j \neq i} \frac{1}{2C_v} \left\{ w^2(r_{ij}) \left[\gamma_{ij}(\vec{e}_{ij} \cdot \vec{v}_{ij})^2 - \frac{\sigma_{ij}^2}{m} \right] - \sigma_{ij} w(r_{ij})(\vec{e}_{ij} \cdot \vec{v}_{ij}) \zeta_{ij} \right\}, \tag{8}$$

$$q_{ij}^R = \sum_{j \neq i} \alpha_{ij} w(r_{ij}) \Delta t^{-1/2} \zeta_{ij}^e, \tag{9}$$

where $r_{ij} = r_i - r_j$ and $v_{ij} = v_i - v_j$; e_{ij} is the unit vector pointing in the direction from j to i. The parameter a_{ij} is a repulsion parameter between the eDPD particles. Also, the γ_{ij} and σ_{ij} in Eqs. (5) and (6) are the strength of dissipative and random forces, respectively. Also, the κ_{ij} and α_{ij} in Eqs. (7) and (9) determine the strength of the collisional and random heat flux. The weight function w decreases monotonically with particle-particle separation distance. It becomes zero beyond the cutoff length and in the present work Lucy weighting function in 2D is used, which is given as

$$w(r_{ij}) = \begin{cases} \frac{5}{\pi} \left(1 + 3\frac{r_{ij}}{r_c} \right) \left(1 - \frac{r_{ij}}{r_c} \right)^3 & (r_{ij} < r_c) \\ 0 & (r_{ij} \geq r_c). \end{cases} \tag{10}$$

The random number ζ_{ij} that appears in Eq. (6) is a random number that has a zero mean and unit variance and has the property $\zeta_{ij} = \zeta_{ji}$ to ensure the conservation of the total momentum of the eDPD system [3–7]. However, the random number ζ_{ij}^e is nonsymmetrical random number with zero mean and unit variance [8,14–17]. The relation between the parameters γ_{ij} and σ_{ij} is governed by the Fluctuation-Dissipation theorem [8,14–17],

$$\gamma_{ij} = \frac{\sigma_{ij}^2(T_i + T_j)}{4k_B T_i T_j}, \tag{11}$$

$$\alpha_{ij} = \sqrt{2k_B \kappa_{ij}} \tag{12}$$

where k_B is the Boltzmann constant. The parameter κ_{ij} is given as

$$\kappa_{ij} = \frac{C_v^2 k_o (T_i + T_j)^2}{4k_B}, \tag{13}$$

where k_o is interpreted as heat friction that controls thermal conductivity [11,12,14,15]. Also, C_v is the heat capacity at constant volume for eDPD particle. In general, the heat capacity of the eDPD particles is normalized by the Boltzmann constant to give a nondimensional number $\bar{C}_v = \frac{C_v}{k_B}$. The mass
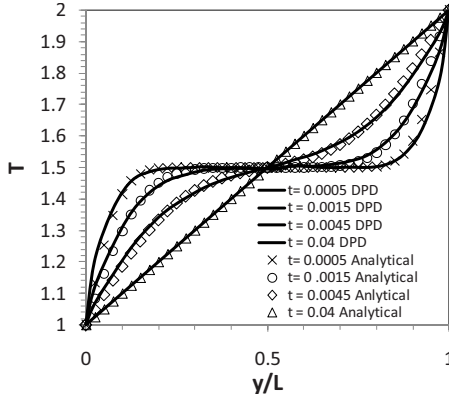
FIG. 1. Temperature evolution in 1D slab: comparison between present eDPD code and analytical solutions.

of eDPD particles and the cutoff radius r_c are set to unity in the entire study.

III. VALIDATION OF THE eDPD CODE

The present eDDP code is validated by simulating two heat transfer problems and comparing the present eDPD results with known analytical and numerical solutions. The first problem of validation is transient heat conduction in a 1D slab governed by the heat equation. This problem was also used for validation by previous researchers [11,12,14,16]. The eDPD particles are uniformly distributed in a 2D lattice where the x and y spacing are taken as $0.5r_c$. To drive the heat transfer a temperature gradient is applied between two given reservoirs, in this case the top and bottom wall of the slab. The top and bottom walls are modeled by two layers of eDPD particles having the same spacing as the interior domain. The temperatures of the bottom and top walls are prescribed, respectively, to 2.0 and 1.0. Also, periodic boundary condition is used in the x direction.

Initially, all of the eDPD particles are assigned an initial temperature of 1.5. The dimensionless heat capacity of the eDPD particles $(\bar{C}_v)$ is set to 1×10^5 and the number density is fixed at 4.0 [14]. The time step is kept very fine ($\Delta t = 0.000\,05$) to capture the evolution of temperature distribution in the domain. The analytical solution is given is [19]

$$T(y,t) = 1 + \frac{y}{L}$$
$$+ \frac{2}{\pi}\sum_{n=1}^{\infty}\frac{2\cos(n\pi)-1}{n}\sin\left(\frac{n\pi y}{L}\right)\exp\left(-\frac{Dn^2\pi^2 t}{L^2}\right)$$
$$- \frac{3}{\pi}\sum_{n=1}^{\infty}\frac{\cos(n\pi)-1}{n}\sin\left(\frac{n\pi y}{L}\right)\exp\left(-\frac{Dn^2\pi^2 t}{L^2}\right),$$
$$(14)$$

where H is the domain height (distance between top and bottom walls) and D is the diffusivity. Figure 1 presents a comparison between eDPD and analytical solution where a good comparison is observed.

The second problem of validation is a simulation of steady state 2D conduction in a slab. This problem has a

fixed form analytical solution and has been used by Chaudhri and Lukes [16] to validate their multicomponent eDPD model. A sketch of the problem geometry and the corresponding boundary condition of this problem are shown in Fig. 2(a). The steady state 2D heat conduction equation is given as [20]

$$\frac{\partial^2 T}{\partial x^2} + \frac{\partial^2 T}{\partial y^2} = 0. \tag{15}$$

The analytical solution of Eq. (15) is given as [20]

$$T(x,y) = \frac{2}{\pi}\sum_{n=1}^{\infty}\frac{(-1)^{n+1}+1}{n}\sin\left(\frac{n\pi x}{H}\right)\frac{\sinh(n\pi y/H)}{\sinh(n\pi W/H)},$$
$$(16)$$

where H and W are the height and width of the slab, respectively, (here $H = W$). The number density is set to 4.0 and the temperatures of the hot and the cold walls are set to 25 and 1.0, respectively. To mimic the large gradients experienced at the wall surfaces, the computation domain is divided into large number of unit cells (40×40) in the x and y directions. However, the use of small number of unit cells (like 10 $\times$ 10) still captures the correct physics of the problem. The following nondimensional temperature is introduced to compare the DPD with the analytical solution,

$$\theta = \frac{T - T_C}{T_H - T_C}, \tag{17}$$

where T is the dimensional temperature and T_C and T_H are the cold and hot temperatures of the reservoirs. The particles are uniformly distributed in the 2D lattice where the x and y spacing are taken as 0.5. All walls are represented by two layers of eDPD particles using the same spacing used as the interior domain. The time step used is 0.000 02. As reflected from Fig. 2(b), that the comparison between the eDPD and analytical solutions is excellent.

The third problem of validation is allocated to test the implementation of the adiabatic boundary condition (i.e.,
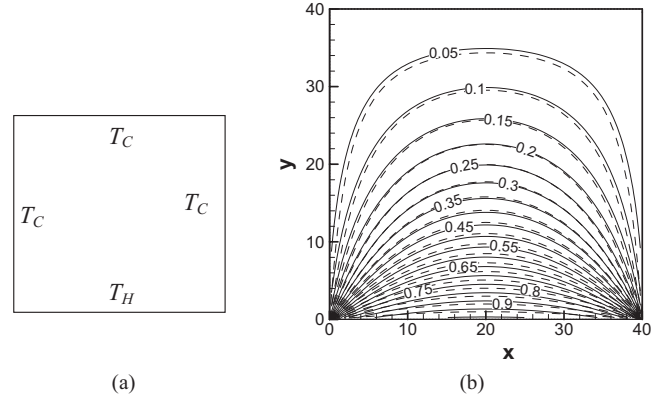

FIG. 2. (a) Sketch of problem geometry for the validation of the 2D eDPD code (b) Temperature isotherms (solid: DPD, dashed dotted: analytical solution).
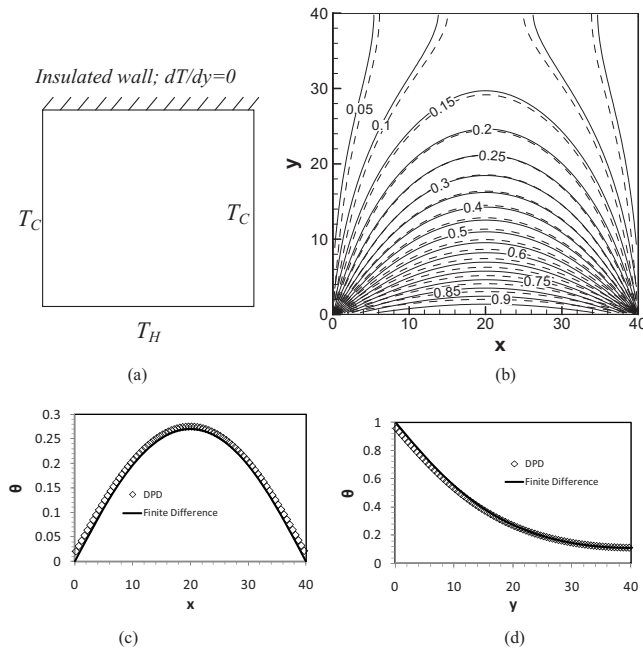
(a)

(b)

(c)

(d)

FIG. 3. Implementation of adiabatic boundary condition (a) Problem geometry (b) temperature isotherms (solid lines: eDPD, dashed lines: analytical solution) (c) Temperature profiles at the midslab height (i.e., $y=20$). (d) Temperature profiles at the midslab width (i.e., $x=20$).

insulated wall) as it will be used later in modeling natural convection. The geometry and the corresponding boundary condition are shown in Fig. 3(a). The left, right, and bottom walls are kept at constant temperature and are treated similar to the top and bottom walls in the previous validation problem. However, the top wall has a different treatment since an adiabatic boundary condition is used. Since an adiabatic boundary condition (zero heat flux, $q_w=0$) means a temperature symmetry condition ($dT/dy=0$), this requires that the distribution of the wall boundary particles to be a mirror image of corresponding particles in the interior eDPD particles. If uniformly distribution particle is used this is automatically satisfied since the same particle spacing is used for the wall eDPD particles as interior particles spacing. However, care must be taken when interior particles are randomly distributed since the location particles in the first layer adjacent to the wall cells has to be saved at and a mirror locations of these particles has to be created to generate the corresponding wall eDPD particles. This is a very essential step in natural convection simulation where all interior eDPD particles are keep moving and therefore the location of the particles in the layers adjacent to the adiabatic wall keep changing with time. In the present work, the algorithm used is constructed such that to check the location of the eDPD particles adjacent to the adiabatic wall and a mirror image of these particles is created in the wall boundary to allocate the wall particles.

Mathematically, the adiabatic boundary condition is given as: $dT/dy=0$. For the present validation problem, a second order accurate forward difference formula for the first derivative at the top wall is expressed as

$$\frac{dT}{dy} = \frac{-3T_{1,j} + 4T_{2,j} - T_{3,j}}{2\Delta y}, \tag{18}$$

where 1, 2, and 3 corresponds to the boundary, first cell and the second cell of the interior domain and Δy is the unit cell width which is equal to unity in the present work. Therefore, solving for the temperature of the boundary, the following formula is obtained,

$$T_{1,j} = \frac{4T_{2,j} - T_{3,j}}{3}. \tag{19}$$

Therefore, the temperature of the wall eDPD particles is expressed in terms of the interior eDPD particles, namely, the first and the second adjacent cells to the wall boundary and the temperature of the wall particles are solved each time step similar to the interior domain particles. The computational domain is divided into large number of unit cells (40 $\times$ 40) in the x and y directions and the time step is similar to the second validation problem (i.e., 0.000 02).

The steady state governing heat conduction equation in 2D is given by Eq. (15). The finite difference (FD) of solution starts with the discritization of Eq. (15) absorbing the boundary conditions shown in Fig. 3(a). The FD solution of this equation (using $\Delta x = \Delta y$) is expressed as [20]

$$T_{mn} = \frac{(T_{m,n+1} + T_{m,n-1} + T_{m+1,n} + T_{m-1,n})}{4}, \tag{20}$$

where the indices m and n designate the x and y in the 2D conduction domain. The temperatures for eDPD and FD solutions are nondimensionalized using Eq. (17). Figures 3(b)–3(d) shows a comparison of eDPD with FD solutions for the temperature isotherms and temperature profiles at midsections in the x and y directions. As revealed from the figure a good comparison is presented. For further validations of the eDPD model, the reader is referred to Abu-Nada [17].

IV. eDPD IMPLEMENTATION AND SOLUTION METHODOLOGY

In this section, the implementation of RB problem and DHE problem in the eDPD model is described in detail. Besides, and the solution procedure is described. Figure 4 shows a schematic diagram of the RB problem and DHE problem. For the RB problem, the distance between the upper cold wall and lower hot wall is defined by H and the width of the top and bottom walls is defined by W. The aspect ratio (i.e., W/H) is kept constant for the present study and is set to the value of 2. The bottom wall is maintained at a hot temperature T_H whereas the top wall is maintained at a cold temperature T_C. However, for the DHE problem, the enclosure is considered square where the aspect ratio is set to unity (i.e., $W/H=1$). The enclosure left wall is maintained at a constant temperature (T_H) higher than the right cold wall temperature (T_C). The upper and the lower walls of the DHE are kept insulated.

The density of the fluid is approximated by the standard Boussinesq model [21]. To facilitate eDPD comparison
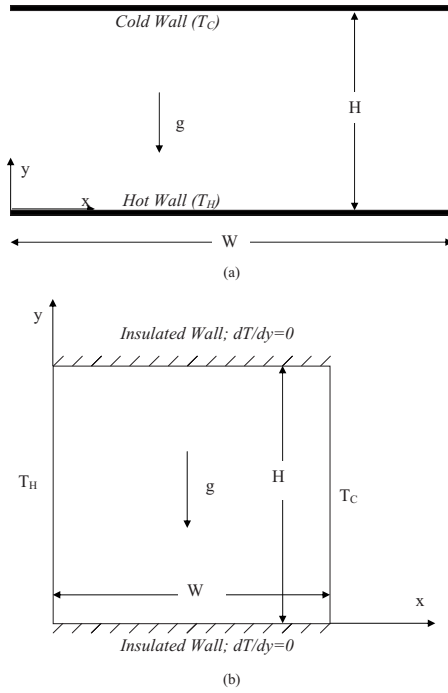
FIG. 4. Schematic of the problems geometries (a) RB problem (b) DHE problem.

against finite volume method, the Navier-Stokes equations are presented first to show that the problems of natural convection in hand are characterized by two important nondimensional numbers, which are Prandtl number (Pr) and Rayleigh number (Ra). Then, the eDPD implementation will be presented. The x and y momentum equations (Navier-Stokes equations) of the flow using the Boussinesq approximation are given as [22]

$$\frac{\partial u}{\partial t} + u\frac{\partial u}{\partial x} + v\frac{\partial u}{\partial y} = -\frac{1}{\rho}\frac{\partial p}{dx} + \nu\left(\frac{\partial^2 u}{\partial x^2} + \frac{\partial^2 u}{\partial y^2}\right), \quad (21)$$

$$\frac{\partial u}{\partial t} + u\frac{\partial v}{\partial x} + v\frac{\partial v}{\partial y} = -\frac{1}{\rho}\frac{\partial p}{dy} + \nu\left(\frac{\partial^2 v}{\partial x^2} + \frac{\partial^2 v}{\partial y^2}\right) + g\beta(T-T_o), \quad (22)$$

where T_o is the reference temperature which is considered as the cold wall temperature (T_C) in the present work. The following dimensionless variables are introduced:

(1) RB problem

$$X = \frac{x}{H}; \quad Y = \frac{y}{H}; \quad U = \frac{u}{\sqrt{g\beta\Delta TH}}; \quad V = \frac{v}{\sqrt{g\beta\Delta TH}};$$

$$P = \frac{p}{\rho_C g\beta\Delta TH}; \quad \theta = \frac{T-T_C}{T_H-T_C}; \quad t' = \frac{t}{H/\sqrt{g\beta\Delta TH}} \quad (23)$$

(2) DHE problem

$$X = \frac{x}{H}; \quad Y = \frac{y}{H}; \quad U = \frac{u}{\alpha_C/H}; \quad V = \frac{v}{\alpha_C/H};$$

$$P = \frac{p}{\rho_C(\alpha_C/H)^2}; \quad \theta = \frac{T-T_C}{T_H-T_C}; \quad t' = \frac{t}{H^2/\alpha_C}, \quad (24)$$

where β is the thermal expansion coefficient, α is the thermal diffusivity, ρ is the density, and the subscript C indicates that the corresponding fluid thermophysical property is evaluated at cold temperature (i.e., T_C). Henceforth, if the subscript C appears it will be indicating that the corresponding fluid thermophysical property is evaluated at cold temperature (i.e., T_C). It is worth mentioning that these are the frequently commonly used nondimensional quantities in literature for both RB and DHE problems. While it is possible to unify both sets of nondimensional quantities presented for the RB and DHE problems, it is decided to keep these two different set of nondimensional quantities to present eDPD values consistent with other values reported in literature.

Using the previous nondimensional quantities, the governing equations are written as

$$\frac{\partial U}{\partial t} + U\frac{\partial U}{\partial X} + V\frac{\partial U}{\partial Y} = -\frac{\partial P}{dX} + \text{Pr}\left(\frac{\partial^2 U}{\partial X^2} + \frac{\partial^2 U}{\partial Y^2}\right), \quad (25)$$

$$\frac{\partial V}{\partial t} + U\frac{\partial V}{\partial X} + V\frac{\partial V}{\partial Y} = -\frac{\partial P}{dY} + \text{Pr}\left(\frac{\partial^2 V}{\partial Y^2} + \frac{\partial^2 V}{\partial Y^2}\right) + \text{Ra Pr } \theta, \quad (26)$$

where the dimensionless numbers are given as

$$\text{Ra} = \frac{g\beta(T_H-T_C)H^3}{\nu_C\alpha_C}; \quad \text{Pr} = \frac{\nu_C}{\alpha_C}. \quad (27)$$

Therefore, the problem of natural convection in DHE is characterized by two basic nondimensional numbers, namely, the Prandtl number (Pr) and the Rayleigh number (Ra). The source term, that is responsible for the fluid movement, is the last term on the right hand side of the y momentum equations [i.e., Ra Pr θ in nondimensional form or $g\beta(T-T_o)$ in the dimensional form].

Now, to model the same kind of physics in the eDPD model one need to implement the same values of Ra and Pr numbers presented in the Navier-Stokes equation. Using the dimensional analysis, the viscous force and the buoyancy force (per unit mass in N/kg) are written, respectively, as

$$f_{viscous} = \alpha\frac{\nu}{H^3}, \quad (28)$$

$$f_{buoyancy} = g\beta\Delta T. \quad (29)$$

So, the ratio of these forces, at reference temperature T_C, is exactly the Rayleigh number as given by Eq. (27). The implementation procedure of Ra and Pr in the eDPD model can be summarized as follows. First, the viscous force is calculated. This is done by calculation of the kinematic viscosity of the eDPD system simply by running a Poiseuille flow. Then, the value of thermal diffusivity will be calculated from the definition of Prandtl number ($\alpha = \nu/\text{Pr}$), where the Pr is set to unity in the entire study. Therefore, for a given value of H the value of the viscous force is known and accordingly the buoyancy force is calculated for a certain value
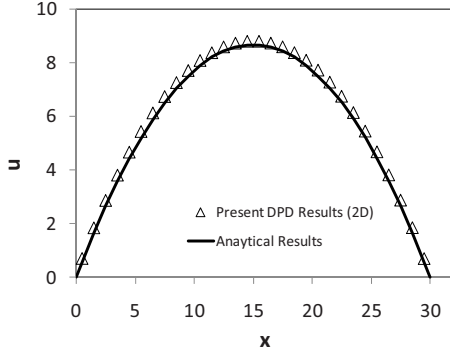
FIG. 5. Validation of Poiseuille flow.

of Rayleigh number (note, $f_{buoyancy} = \text{Ra} \times f_{viscous}$). Once the buoyancy force is known the value of the quantity $(g\beta)$ in Eq. (2) becomes a known quantity for a given ΔT. The next paragraph will present implementation details this procedure.

Thus, the first task toward simulation of natural convection to evaluate the kinematic viscosity and thermal diffusivity of the eDPD system using prescribed eDPD parameters (such as σ_{ij}, γ_{ij}, a_{ij}, k_o). It is important to note that the thermal diffusivity and kinematic viscosity are evaluated at cold temperature since the Rayleigh number and the Prandtl number are defined at cold conditions (i.e., $T_C = 1.0$) or at $k_b T = 1.0$ in eDPD context.

In the present work the kinematic viscosity is measured first by running a Poiseuille flow between parallel plates (using $k_b T = 1$) where a periodic boundary condition is applied at inlet/outlet and no-slip boundary condition is applied at the plates. To drive the flow a constant body force, in the x direction, is applied at each DPD particle. A problem with a domain size of 30×30 is simulated and the body force is set to 0.02. The number density is taken as 4.0 and the other DPD parameters used are: $\sigma_{ij} = 3$, $\gamma_{ij} = 4.5$, $a_{ij} = 18.75$. No-slip boundary condition is used at the top and bottom walls (details of boundary conditions implementation will be discussed later in this section). For the present simulation, the maximum velocity obtained is 8.78. The steady state solution of the Poisuielle flow is given by the analytical solution

$$u(x) = \frac{\rho F_p h^2}{8\mu} \left[\frac{y}{h} - \left(\frac{y}{h} \right)^2 \right], \quad (30)$$

where μ is the dynamic viscosity which is related to kinematic viscosity by the relations $(\mu = \rho\nu)$ and F_p is the constant body force.

As shown from the previous relation that the maximum velocity is given as $u_{\max} = \frac{\rho F_p h^2}{8\mu}$. The maximum velocity from the present simulation is found 8.78 and using the above mentioned parameters (i.e., $F_p = 0.02$, H = 30, $\rho = 4$), the value of the kinematic viscosity is found 0.265. This maximum velocity is slightly higher than other values reported by other researchers who used three-dimensional (3D) simulation of the DPD simulations (for example, a value of 8.639 was reported by Fan *et al.* [7]) and this difference (around 1.6%) is related to the fact that the present eDPD model is 2D whereas the 8.639 value was obtained from a 3D DPD model. Figure 5 shows such a comparison between the

present 2D and analytical solution given in Eq. (30) using the 3D maximum velocity, $u_{\max} = 8.639$.

After estimating the value of the kinematic viscosity (using $\sigma_{ij} = 3$, $\gamma_{ij} = 4.5$, $a_{ij} = 18.75$, which will be kept constant hereafter), the thermal diffusivity was simply prescribed from the definition of the Prandtl number,

$$\alpha = \frac{\text{Pr}}{\nu}. \quad (31)$$

In the present study, the value of Pr is set to unity. Therefore, the value of thermal diffusivity is equal to kinematic viscosity. However, to understand the procedure of setting this value of thermal diffusivity to the eDPD model, more details are given hereafter.

By looking at the eDPD equations, given by Eqs. (4)–(13), it is noticed that the thermal diffusivity is not an input parameter, but it can be compiled from other eDPD parameters such as κ_{ij} (or the heat friction parameter, k_o). Therefore, to set the thermal diffusivity of the eDPD system to 0.265 (i.e., Pr=1), we run a transient simulation of heat conduction in a 2D slab having one wall maintained at hot temperature and other walls kept at cold temperature as shown in Fig. 6(a). We started with a guess value of k_o (calculated from the kinetic theory presented by Ripoll [23]) to run this eDPD simulation. Details of k_o calculations are given in the Appendix. To check if obtained eDPD temperature distribution in the slab using this guess value of k_o match to the required value of thermal diffusivity of the eDPD system (i.e., 0.265), the same problem is recalculated using the FD method. The governing equation for transient heat conduction in 2D is given as

$$\frac{1}{\alpha} \frac{\partial T}{\partial t} = \frac{\partial^2 T}{\partial x^2} + \frac{\partial^2 T}{\partial y^2}. \quad (32)$$

The FD solution of this equations (using $\Delta x = \Delta y$) is expressed as

$$T_{m,n}^{t+\Delta t} = \frac{\alpha \Delta t}{(\Delta x)^2} (T_{m,n+1}^t + T_{m,n-1}^t + T_{m+1,n}^t + T_{m-1,n}^t)$$

$$+ \left(1 - 4 \frac{\alpha \Delta t}{(\Delta x)^2} \right) T_{mn}^t, \quad (33)$$

where the indices m and n designate the x and y in the 2D slab.

The same conditions of the eDPD problem are solved by the FD approach, i.e., same problem geometry [Fig. 6(a)], same initial conditions, same boundary conditions, same domain size, and same total running time of simulation. After running the FD solution for 40 000 time steps, the finite difference solution is obtained. The FD temperature distribution in the slab obtained after 40 000 is plotted on top of the eDPD temperature distribution and from the comparison of the both temperature distribution it is possible to judge if the thermal diffusivity of eDPD system corresponds exactly to the 0.265. It was found the guess value of k_o will lead the
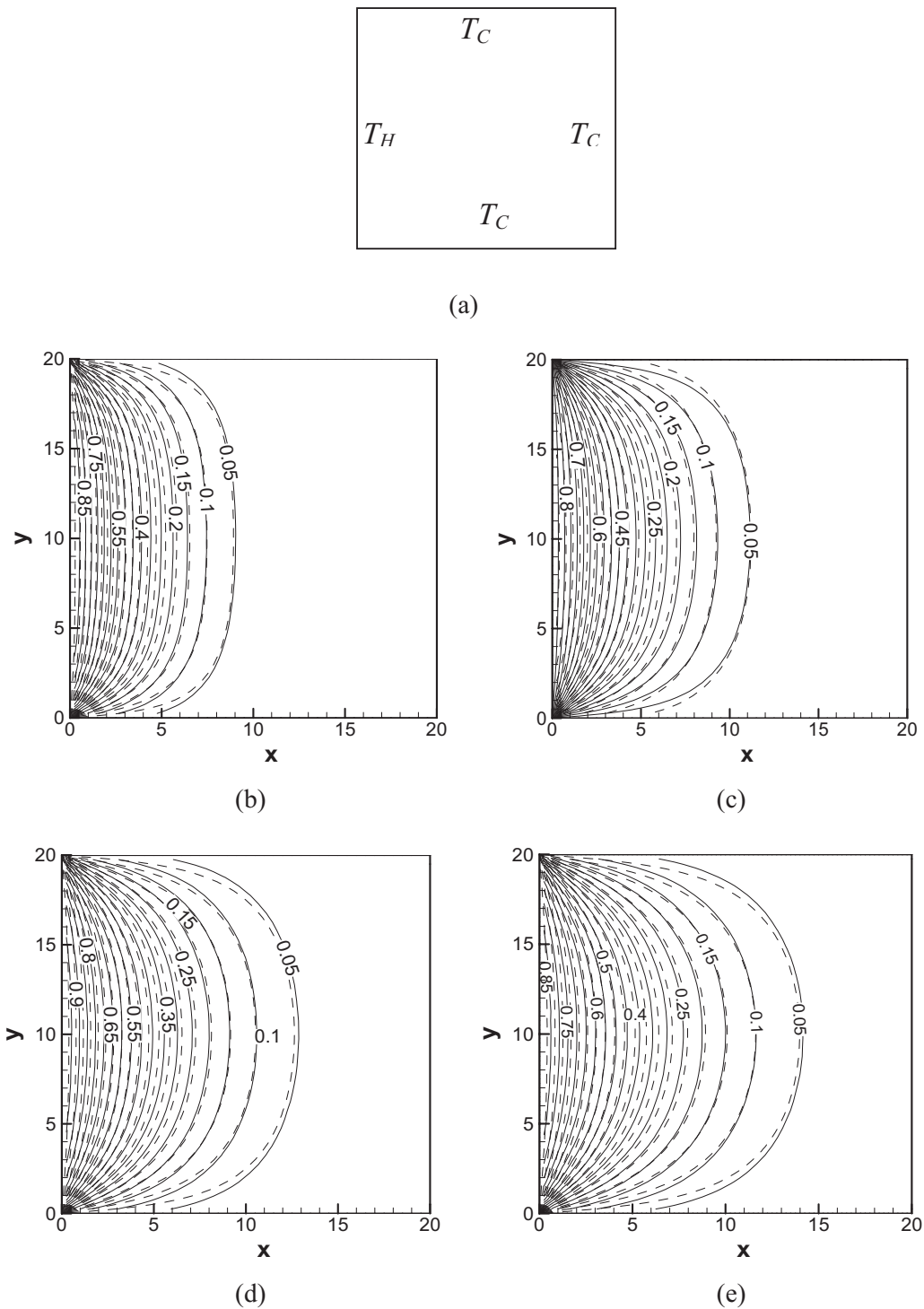
FIG. 6. Calculation of thermal diffusivity; FD solutions (dashed lines) and eDPD solution (solid lines) (a) Problem geometry (b) snapshot of temperature distribution at $t=40\,000$ (b) snapshot of temperature distribution at $t=60\,000$. (c) snapshot of temperature distribution at $t=80\,000$ (d) snapshot of temperature distribution at $t=100\,000$.

temperature distribution of the eDPD solution to spread (diffuse) faster or slower than the FD solution, which means that this guess value corresponds to a higher or lower thermal diffusivity than the required eDPD diffusivity. Therefore, the value of k_o is turned until both FD and eDPD solutions match. For the present comparison, both solutions are shown to match by having k_o equal to 0.000 126; see Fig. 6(b).

Therefore, this is the required k_o that corresponds to a diffusivity of 0.265 (i.e., Pr=1.0). The eDPD simulations continued with this value of k_o for 60 000, 80 000, and 100 000 time steps and a comparison between the FD and eDPD solutions is given in Figs. 6(b)–6(d). As shown from the figure a good match between both approaches is registered using k_o=0.000 126. This value of thermal diffusivity was further

checked by means of mesoscopic heat flux calculation given by Ripoll *et al.* [11]

$$q = \sum_{j \neq i} \kappa_{ij} w(r_{ij}) \left(\frac{1}{T_i} - \frac{1}{T_j} \right) \vec{r}_{ij}. \qquad (34)$$

The thermal conductivity was calculated by means of the Fourier's law, $k = -\frac{q}{\partial T / \partial x}$, where the temperature gradient is given as $(\Delta T / \Delta L)$. After getting the value of the thermal conductivity from this approach, it is divided by (ρC_v) to get the thermal diffusivity. It was found that the value of thermal diffusivity obtained from this k_o was 0.2648, which is in excellent agreement of 0.265 from the first approach. This gives a confidence on the value estimation the value of thermal diffusivity.

After solving for the thermal diffusivity and kinematic viscosity, then using prescribed values of Ra, H, and ΔT the buoyancy and viscous forces become known quantities and accordingly the quantity $(g\beta)$ is determined which completes all parameters needed to run the eDPD simulation of the RB and DHE problems. Table I presents full details of eDPD parameters used to run natural convection for the whole range of Rayleigh numbers for the present study.

The Groot-Warren method is used to solve the eDPD equations [3]. The implementation of this method is summarized as follows:

Step 1:$x^{n+1} = x^n + \Delta t u^n + \frac{1}{2}(\Delta t)^2 f_x^n,$

$$y^{n+1} = y^n + \Delta t v_\eta^n + \frac{1}{2}(\Delta t)^2 f_y^n, \qquad (35)$$

Step 2:$\tilde{u}^{n+1} = u^n + \frac{1}{2}(\Delta t) f_x^n,$

$$\tilde{v}^{n+1} = v^n + \frac{1}{2}(\Delta t) f_y^n,$$

$$\tilde{T}^{n+1} = \tilde{T}^n + \frac{1}{2\overline{C_v}}(\Delta t) q^n, \qquad (36)$$

Step 3:$f_x^{n+1} = f_x^n(x^{n+1}, y^{n+1}, \tilde{u}^{n+1}, \tilde{T}^{n+1}),$

$$f_y^{n+1} = f_y^n(x^{n+1}, y^{n+1}, \tilde{v}^{n+1}, \tilde{T}^{n+1}),$$

$$q^{n+1} = q^n(x^{n+1}, y^{n+1}, \tilde{v}^{n+1}, \tilde{T}^{n+1}), \qquad (37)$$

Step 4:$u^{n+1} = u^n + \frac{1}{2}\Delta t(f_x^{n+1} + f_x^n),$

$$v^{n+1} = v^n + \frac{1}{2}\Delta t(f_y^{n+1} + f_y^n),$$

$$T^{n+1} = T^n + \frac{1}{2\overline{C_v}}\Delta t(q^{n+1} + q^n). \qquad (38)$$

It is worth mentioning that recent studies of Besold *et al.* [24] and Nikunen *et al.* [25] and discussed more accurate

TABLE I. eDPD parameters (for both RB and DHE).

Ra	5×10^4
Pr	1
γ	4.5
σ	3
ν	0.265
α	0.265
ρ	4
k_o	0.000126
$g\beta$	0.22
Total number of iterations	2×10^5
Number of iteration for statistical averaging	5×10^4
T_H	1.4
T_L	1.0
H	20
Δt	0.02

integration schemes for the DPD thermostat equations.

The velocity boundary conditions used are the no-slip boundary condition, and the specular boundary conditions. Starting with the DHE problem, the no-slip boundary condition was implemented on the whole enclosure walls by following the approach proposed by Fan *et al.* [7] and Duong-Hong *et al.* [26] by implementing two layers of frozen particles. To avoid the penetration of fluid particles the solid walls, the particles are bounded back according to the following formula (Fan *et al.* [7], Duong-Hong *et al.* [26])

$$\vec{r}_{new} = \vec{r}_{new} + 2d_r\vec{n}_w, \qquad (39)$$

where d_r is the distance from the particle to the boundary and $\vec{n}_w$ is a normal unit vector on the wall directing in the direction of inner fluid domain. The bounced back particles has the velocities

$$\vec{V}_{new} = 2\vec{V}_{wall} - \vec{V}_{old}. \qquad (40)$$

However, for the RB problem half of the domain is solved due to the symmetry experienced in the problem. This has the advantage of reducing computational time in half.

The left and right boundaries are treated as symmetry boundaries as shown in Fig. 7(a). The specular reflection boundary condition is adopted in the current study to represent the symmetry boundary condition and it is considered the most commonly used boundary condition for symmetry boundary conditions in particle simulations [27,28]. The line of symmetry particles distribution are treated exactly as the adiabatic wall particles where they are considered as mirror images of the particles in the first cell adjacent to the line of symmetry [see Fig. 7(b)]. When implementing the specular reflection model, the normal component of the momentum for eDPD particles colliding with the line of symmetry is reversed, while the component parallel to the line of symmetry is not changed.

Regarding the temperature boundary condition, a constant temperature boundary condition is prescribed on the left and the right walls and zero heat flux (i.e., $dT/dy = 0$) on the top
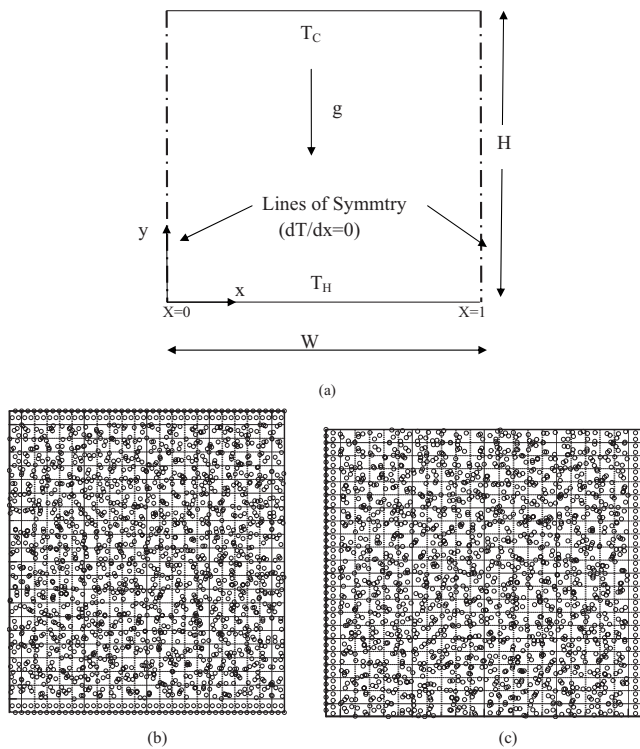
FIG. 7. (a) RB solution domain and corresponding boundary conditions (b) Distribution of eDPD particles for the RB problem (c) Distribution of eDPD particles for the DHE problem.

and the bottom walls. The same procedure outlined for the second validation problem is adopted for the top and bottom walls of the DHE. The boundary particles distribution are considered as mirror images of the particles in the first cell adjacent to the line of symmetry [see Fig. 7(b)].

V. SIMULATION RESULTS OF THE RB PROBLEM

In this section, the problem of Rayleigh-Bénard (RB) problem is studied using the eDPD approach and the results are compared to finite volume (FV) solutions at steady state. The FV solution procedure is not described in this paper and the reader is referred to the work of Abu-Nada *et al.* [18] and Abu-Nada and Öztop [22] for full description of the solution procedure. It is worth mentioning that the solution of the RB is conducted only for the range $(0 \le X \le 1)$ due to the symmetry and at the end of the simulation the results for the range $(1 \le X \le 2)$ is obtained as a mirror image of the results presented for $(0 \le X \le 1)$.

The Rayleigh-Bénard (RB) thermo convection problem is driven by the buoyancy effects when a fluid is confined between two horizontal (hot and cold) plates having a temperature difference ΔT. For this problem, if the Ra number is greater than 1707, then thermo convective fluid motion is initiated between the plates and the heat transfer is no longer dominated by conduction. This convection motion develops a thermal plume with two adjacent fluid rolls rotating in opposite directions. The strength of the convection currents increase by increasing the Rayleigh number and the shape of the plume becomes very clear as the Rayleigh number is increasing.
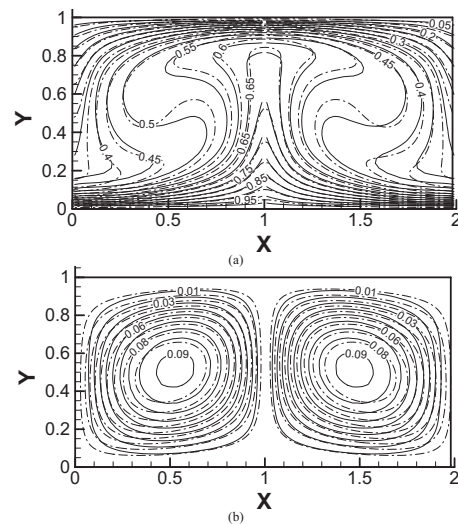

FIG. 8. (a) Temperature isotherms for RB (solid lines: eDPD, dashed dotted lines: FV solution) (b) Streamlines for RB (solid lines: eDPD, dashed dotted lines: FV solution).

increasing. For the present work, the Rayleigh number is set to 4.5×10^4 to guarantee a distinct appearance of the thermal plume.

Figure 8(a) illustrates the temperature isotherms and streamlines for the RB problem under study where it is shown on the same figure both the eDPD and FV solutions. As shown from the isotherms the basic feature of RB problem are depicted accurately by the eDPD, such as the appearance of the thermal plume and the two thermal boundary layers at the top and the bottom plates. Besides, it is shown that next to the walls the temperature isotherms are almost horizontal, which demonstrates the dominance of the conduction heat transfer next to the walls whereas in the region between the plates the temperature isotherms are no longer horizontal due to the dominance of convection. It is clearly shown that a good match between the eDPD results and the FV results is observed. Also, the two rotating rolls are clearly demonstrated by the streamlines as shown in Fig. 8(b). The vector plots portrayed in Fig. 9 shows the direction of rotation of the circulation rolls.

Figure 10 illustrates temperature and velocity profiles for the RB problem. Three profiles at three different sections along the heated wall are shown [at $X=1$ (centerline of plume), $X=0.5$ (midsolution section), and $X=0$ (line of symmetry); see Fig. 7(a)]. Also, on the same figure the temperature profiles (dashed dotted lines) using FV solutions are shown. The figure shows that the temperature gradient at the bottom heated wall is minimum in the plume regions, which is a basic feature of the heat transfer in RB problem and this is predicted correctly by the eDPD simulation since the difference between the eDPD and the finite volumes is relatively small. Also, Fig. 10(b) shows the V velocity at the same three mentioned planes where the exact trend is observed. However, some deviation is observed at the $X=1$ and $X=0$ and the maximum difference occurs around the middistance between the plates. Also, the same conclusion is observed for the U velocity; however, a good match is observed at $X=0.5$.
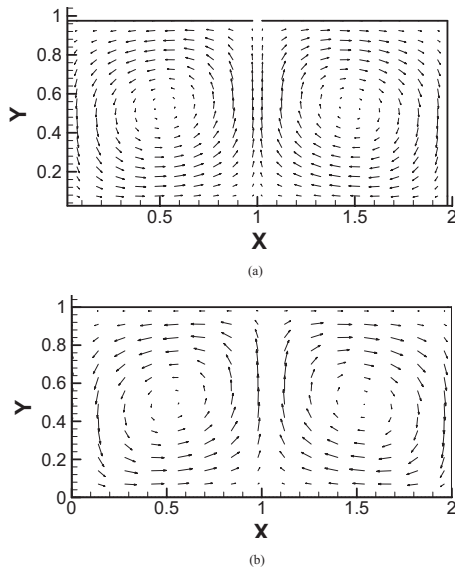
FIG. 9. RB vector plots (a) eDPD (b) FV solution.

To have a thorough picture to the velocities (U and V) distribution throughout the RB problem domain, Fig. 11 is presented and as shown a good match between the FV and eDPD throughout the flow domain. However, the maximum deviation in velocity is observed near the mid-distance between the plates and at the lines of symmetry. To have a more insight of the temperature and velocities at the mid-distance, Fig. 12 is presented and it is clear that the V-velocity deviation is maximum next to the lines of symmetry. This difference is related to the accuracy of specular boundary condition (the condition employed in the current formulation) in resembling the symmetry boundary. However, overall assessment tells that the prediction of the eDPD is good and the all features of the RB problem are predicted properly.

To test the effect of the symmetry boundary condition, the same RB problem is solved using the full domain ($0 \leq X \leq 2$) where a periodic boundary condition at the inlet/outlet of the domain is employed instead of the specular boundary condition. A snapshot of the isotherms and the streamlines are shown in Fig. 13 where a reasonable prediction of the RB is observed at $t = 33\,000$. However, this kind of boundary condition did not lead to steady state solution where a kind of "diffusion" of the plume occurred at later stages of simulation and the exact plume shape disappears as time progressing as shown by the snapshot observed at simulation time $= 100\,000$. Therefore, this boundary condition did not help in maintaining the RB at steady state and this is the reason for using the specular boundary condition to represent the symmetry boundary condition.

VI. SIMULATION OF THE DHE PROBLEM

In this section, the problem of differentially heated enclosure (DHE) is studied using the eDPD approach and the results are compared to finite volume (FV) solutions at steady state. Figure 14 illustrates temperature profiles from the present eDPD for the DHE problem. Three profiles at three
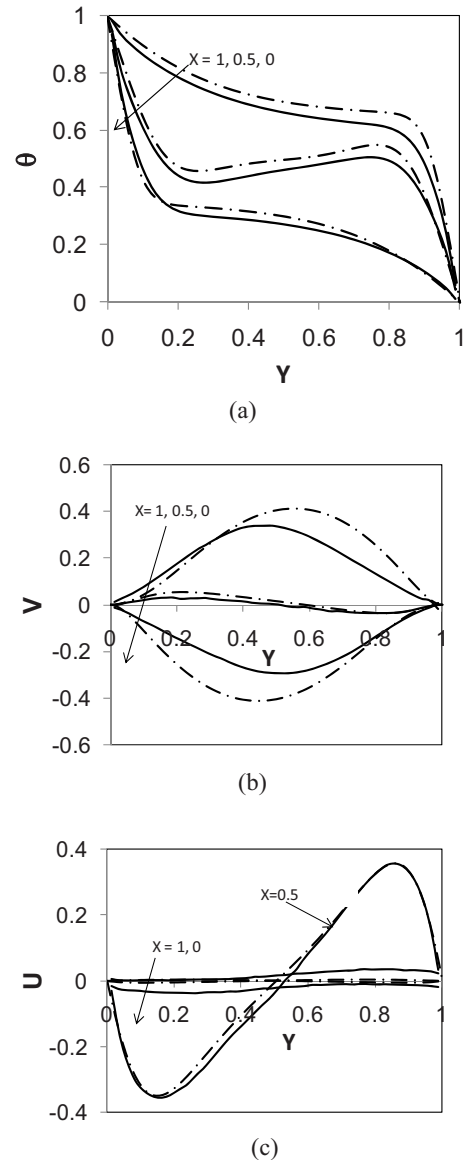

FIG. 10. RB profiles at three different sections of the heated wall (solid lines: eDPD, dashed dotted lines: FV solution) (a) temperature; (b) V velocity; (c) U velocity.

different sections along the heated wall are shown (i.e., $Y = 0.25$, $Y = 0.5$ (midsection), and $Y = 0.75$). Also, on the same figure the temperature profiles (dashed lines) using FV solutions are shown. The figure shows that the temperature gradient at the heated wall (along the y direction) decrease due to the increased thickness of the thermal boundary layer, which is a basic feature of the heat transfer in differentially heated enclosures and this is predicted properly by the eDPD simulation since the difference between the eDPD and the finite volumes is relatively small. Also, Fig. 14 shows how the temperature distribution becomes nearly uniform in the inner of the enclosure which is due to dominance of convection.

A more insight in the temperature distribution all over the enclosure is revealed by plotting temperature isotherms in the enclosure using the eDPD (the solid lines) and the FV solutions (the dashed dotted lines) as demonstrated in Fig.
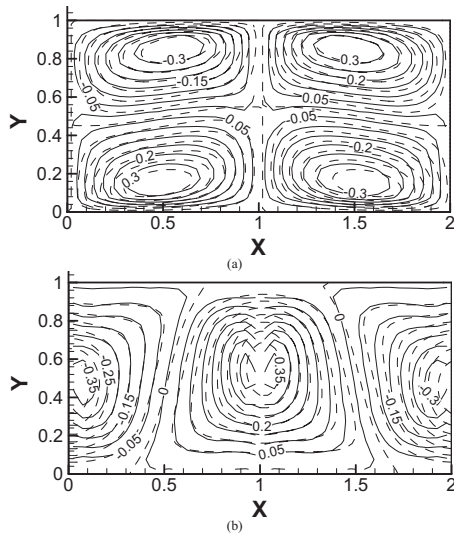
FIG. 11. RB velocity contours (solid lines: eDPD, dashed dotted lines: FV solution) (a) U velocity; (b) V velocity.

15(a). As shown, a good match between both methods is observed. Moreover, the basic features of heat transfer in differentially heated enclosures are all captured by the eDPD simulation. For example, for this Rayleigh number the isotherms become almost vertical near the hot and cold walls and horizontal in the middle of the enclosure due to the dominance of convection. Also, the figure shows clearly the thermal boundary layers at both hot and cold walls. To have a better insight of the flow field inside the enclosure, the velocity streamlines are presented in Fig. 15(b). It is revealed

(a)

(b)
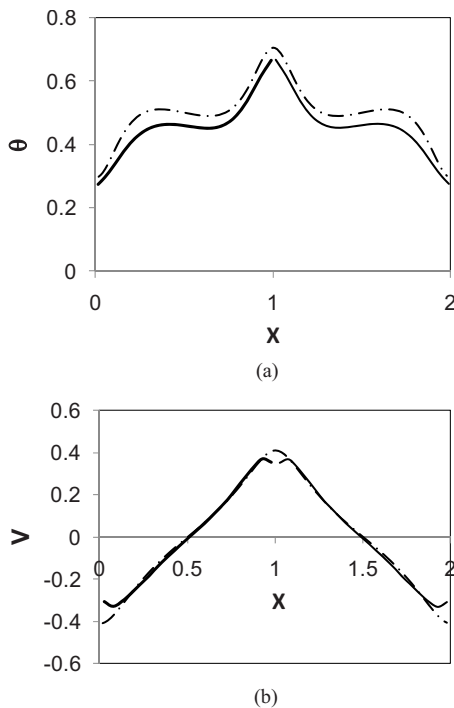
FIG. 12. RB Profiles at the mid-distance between the hot and the cold wall (solid lines: eDPD, dashed dotted lines: FV solution) (a) temperature; (b) V velocity
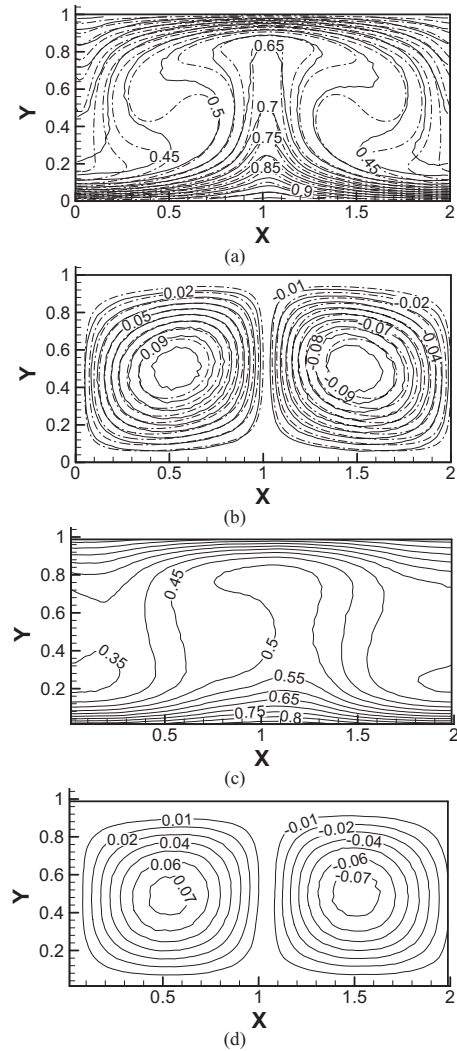
FIG. 13. RB simulation using full domain and periodic boundary condition at inlet/outlet (a) isotherms $t=33\,000$ (b) streamlines $t=33\,000$ (c) eDPD isotherms $t=100\,000$ (d) eDPD streamlines $t=100\,000$.

from the figure that a single circular circulation cell is located at the center of the enclosure by the eDPD simulations and the direction of circulation is clockwise, where the main cell consists of two small counter rotating smaller cells at the ends of the main cell as shown from the vector plots given in
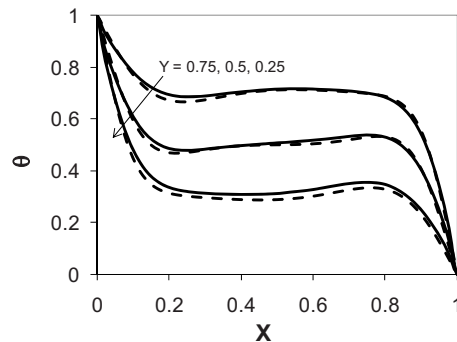

FIG. 14. DHE temperatures profiles at three different sections of the heated wall (solid lines: eDPD, dashed lines: FV solution).
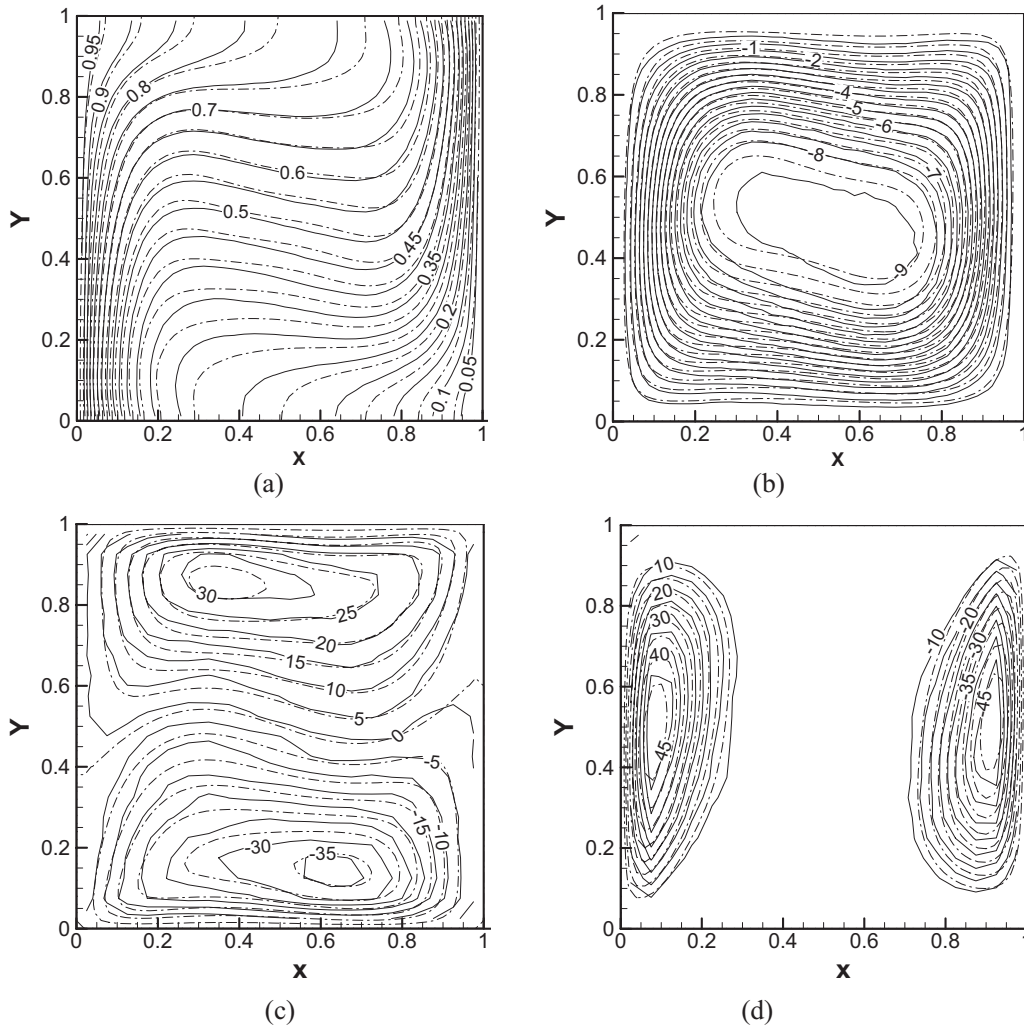
FIG. 15. DHE contours (solid lines: eDPD, dashed dotted lines: FV solution) (a) temperature isotherms (b) streamlines; (c) U velocity; (d) V velocity.

Fig. 16. Also, Figs. 15(c) and 15(d) show the good match between the eDPD and the FV as depicted in the *U* and *V* velocity contours.

Figure 17 shows details of the nondimensional velocity profiles. The figures illustrate an excellent match between the eDPD and the FV solution. Figure 17 shows how the velocities are minimal in the middle of the enclosure and this is due to the circulation cell (see Figs. 15 and 16) encountered in the middle of the channel. Also, Fig. 17 demonstrates how the boundary layer velocity profiles are clearly distinguished. These figures again support the capability of the eDPD approach to model natural convection in differentially heated enclosures and to capture important physical features of the problem.

After solving for the velocity and temperature fields more useful quantities for engineering applications are obtained. For example, the Nusselt number can be expressed as

$$\mathrm{Nu} = \frac{hH}{k}. \tag{41}$$

The heat transfer coefficient is computed from

$$h = \frac{q_w}{T_H - T_C}. \tag{42}$$

The thermal conductivity of is expressed as

$$k = -\frac{q_w}{\partial T/\partial n}. \tag{43}$$

Plugging the expression of *h* given in Eq. (42) and the expression of *k* given in Eq. (43) in Eq. (41), then the Nusselt number is expressed as

$$\mathrm{Nu} = -\frac{H}{(T_H - T_L)}\frac{\partial T}{\partial n}. \tag{44}$$

Therefore, to plot the Nusselt number we need to calculate the temperature gradient. The temperature gradient term in Eq. (44) is evaluated at the hot walls of the DHE or the RB and expressed by a second order accurate forward differencing formula as
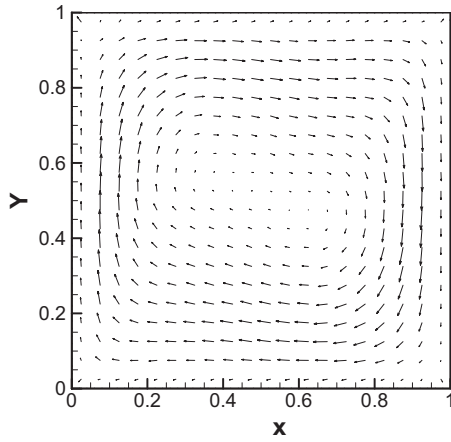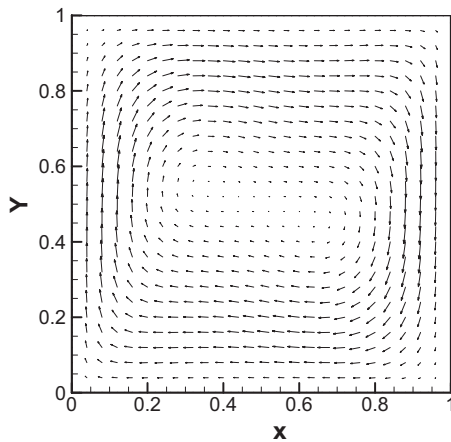
FIG. 16. Vector plots for the DHE problem (a) eDPD (b) FV solution.

$$\frac{dT}{dx'} = \frac{-3T_1 + 4T_2 - T_3}{2\Delta n},$$ (45)

where 1, 2, and 3 are the wall, first bin adjacent to the wall, and second bin adjacent to the wall. Figure 18 shows the distribution of Nusselt number along the heated wall for the DHE and RB problem. Generally speaking, there is a good match between the FV and the eDPD where the trend is clearly demonstrated.

VII. CONCLUSIONS

Dissipative particle dynamics with energy conservation (eDPD) was applied to investigate 2D natural convection RB problem and DHE problem. The eDPD simulations were benchmarked against finite volume solutions and it was found that eDPD appropriately predict the temperature and flow fields correctly in natural convection. The eDPD temperature and velocity fields agree with the finite volume solutions. The outcome of this study is very helpful for future studies concerned with heat transfer enhancement in natural convection using nanoparticles.
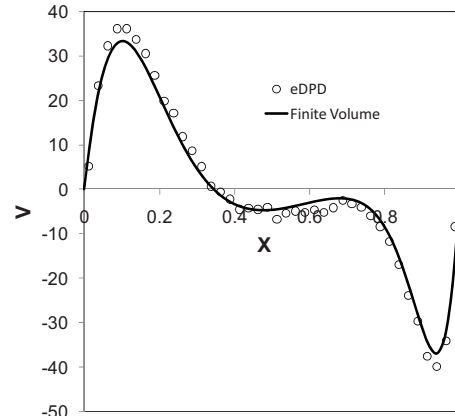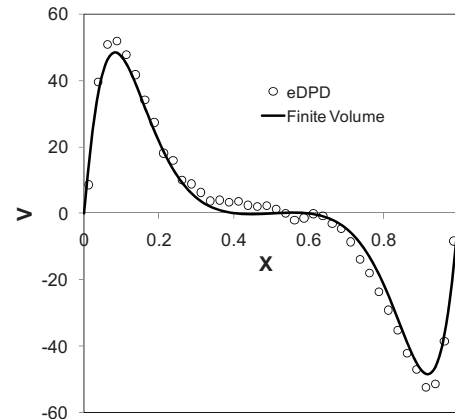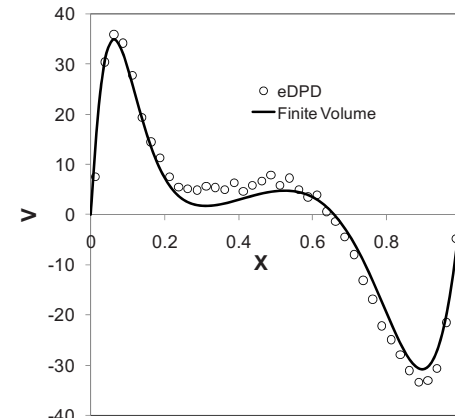
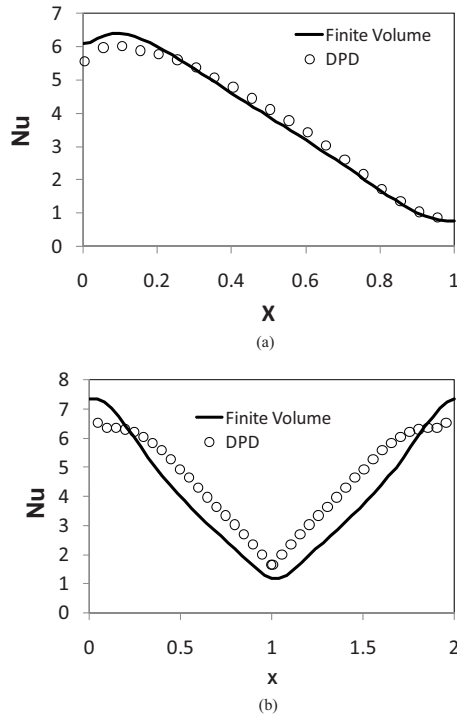FIG. 17. DHE Velocity profiles (a) $Y = 0.25$; (b) $Y = 0.5$; (c) $Y = 0.75$.

FIG. 18. Nusselt number distribution along the heated wall (a) DHE and (b) RB.

APPENDIX

This relations given by Ripoll [23] is given as

$$\alpha = \frac{k}{\rho C_v} = \frac{(d+3)}{2(d+5)(d+6)} \omega_e r_c^2, \tag{A1}$$

where k is the thermal conductivity, d is the dimension, which is equal to 2 in the present work since we are simulating 2D eDPD system.

The parameter ω_e is the collision frequency and it is given as [23]

$$\omega_e = \bar{C}_v \rho [w] k_o, \tag{A2}$$

where

$$[w] = \int_0^1 w(r_{ij}) dr. \tag{A3}$$

Therefore, we can rearrange the Ripoll formula in the following form:

$$\omega_e = \frac{2\alpha(d+5)(d+6)}{(d+3) r_c^2}. \tag{A4}$$

Substituting the relation of collision frequency, given by Eq. (A2), then we can solve for the heat friction parameter k_o which is written as

$$k_o = \frac{\dfrac{2\alpha(d+5)(d+6)}{(d+3) r_c^2}}{\bar{C}_v \rho [w]}. \tag{A5}$$

Since, all parameter in the right-hand side of Eq. (A5) are known, therefore, the value of k_o can be calculated.

[1] P. J. Hoogerbrugge and J. M. V. A. Koelman, Europhys. Lett. **19**, 155 (1992).

[2] T. Murtola, A. Bunker, I. Vattulainen, and M. Deserno, Phys. Chem. Chem. Phys. **11**, 1869 (2009).

[3] R. D. Groot and P. B. Warren, J. Chem. Phys. **107**, 4423 (1997).

[4] P. Español and P. Warren, Europhys. Lett. **30**, 191 (1995).

[5] C. A. Marsh, G. Backx, and M. Ernst, Phys. Rev. E **56**, 1676 (1997).

[6] R. D. Groot and K. L. Rabone, Biophys. J. **81**, 725 (2001).

[7] X. J. Fan, P. T. Nhan, T. Y. Ng, X. H. Wu, and D. Xu, Phys. Fluids **15**, 11 (2003).

[8] P. Español, Europhys. Lett. **40**, 631 (1997).

[9] J. B. Avalos and A. D. Mackie, Europhys. Lett. **40**, 141 (1997).

[10] L. Pastewka, D. Kauzlarić, A. Greiner, and J. Korvink, Phys. Rev. E **73**, 037701 (2006).

[11] M. Ripoll, P. Español, and M. H. Ernst, Int. J. Mod. Phys. C **9**, 1329 (1998).

[12] M. Ripoll and P. Español, Heat Technol. **18**, 57 (2000).

[13] A. D. Mackie, D. Bonet, J. B. Avalos, and V. Navas, Phys. Chem. Chem. Phys. **1**, 2039 (1999).

[14] R. Qiao and P. He, Mol. Simul. **33**, 677 (2007).

[15] P. He and R. Qiao, J. Appl. Phys. **103**, 094305 (2008).

[16] A. Chaudhri and J. R. Lukes, ASME J. Heat Transfer **131**, 033108 (2009).

[17] E. Abu-Nada, Mol. Simul. **36**, 382 (2010).

[18] E. Abu-Nada, Z. Masoud, H. Oztop, and A. Campo, Int. J. Therm. Sci. **49**, 479 (2010)

[19] H. S. Carslaw and J. C. Jaeger, *Conduction of Heat in Solids*, 2nd ed. (Oxford University Press, New York, 1986).

[20] F. P. Incropera and D. P. Dewitt, *Introduction to Heat Transfer*, 3rd ed. (Wiley, New York, 1996).

[21] E. Abu-Nada and H. Oztop, Int. J. Heat Fluid Flow **30**, 669 (2009).

[22] F. White, *Vsicous Fluid Flow*, 2nd ed. (McGraw-Hill, New York, 1991).

[23] M. Ripoll, Ph.D. thesis, Universidad Nacional de Educación a Distancia, Madrid, 2002.

[24] G. Besold, I. Vattulainen, M. Karttunen, and J. M. Polson, Phys. Rev. E **62**, R7611 (2000).

[25] P. Nikunen, M. Karttunen, and I. Vattulainen, Comput. Phys. Commun. **153**, 407 (2003).

[26] D. Duong-Hong, N. Phan-Thien, and X. Fan, Comput. Mech. **35**, 24 (2004).

[27] P. Szymczak and A. J. C. Ladd, Phys. Rev. E **68**, 036704 (2003).

[28] G. H. Cottet and P. D. Koumoutsakos, *Vortex Methods: Theory and Practice* (Cambridge University Press, Cambridge, England, 2000).